

Orbital angular momentum comb generation from azimuthal binary

phases: Supplementary Materials

Shiyao Fu^{1,2,3,*}, Zijun Shang^{1,2,3}, Lan Hai^{1,2,3}, Lei Huang^{1,2,3}, Yanlai Lv^{1,2,3},
and Chunqing Gao^{1,2,3,**}

1 School of Optics and Photonics, Beijing Institute of Technology, Beijing 100081, China

*2 Key Laboratory of Information Photonics Technology, Ministry of Industry and Information Technology of the
People's Republic of China, Beijing 100081, China*

*3 Key Laboratory of Photoelectronic Imaging Technology and System, Ministry of Education of the People's
Republic of China, Beijing 100081, China*

* *fushiyao@bit.edu.cn*

** *gao@bit.edu.cn*

Supplementary Note 1: Diffractions of azimuthal binary phase

Azimuthal binary phase grating is a phase-only grating with periodically various phases along the azimuth direction. As shown in Fig. S1, the grating has azimuthal transition points along the azimuth direction, and there is a phase jump of $0 \sim \pi$ or $\pi \sim 0$ at each transition point.

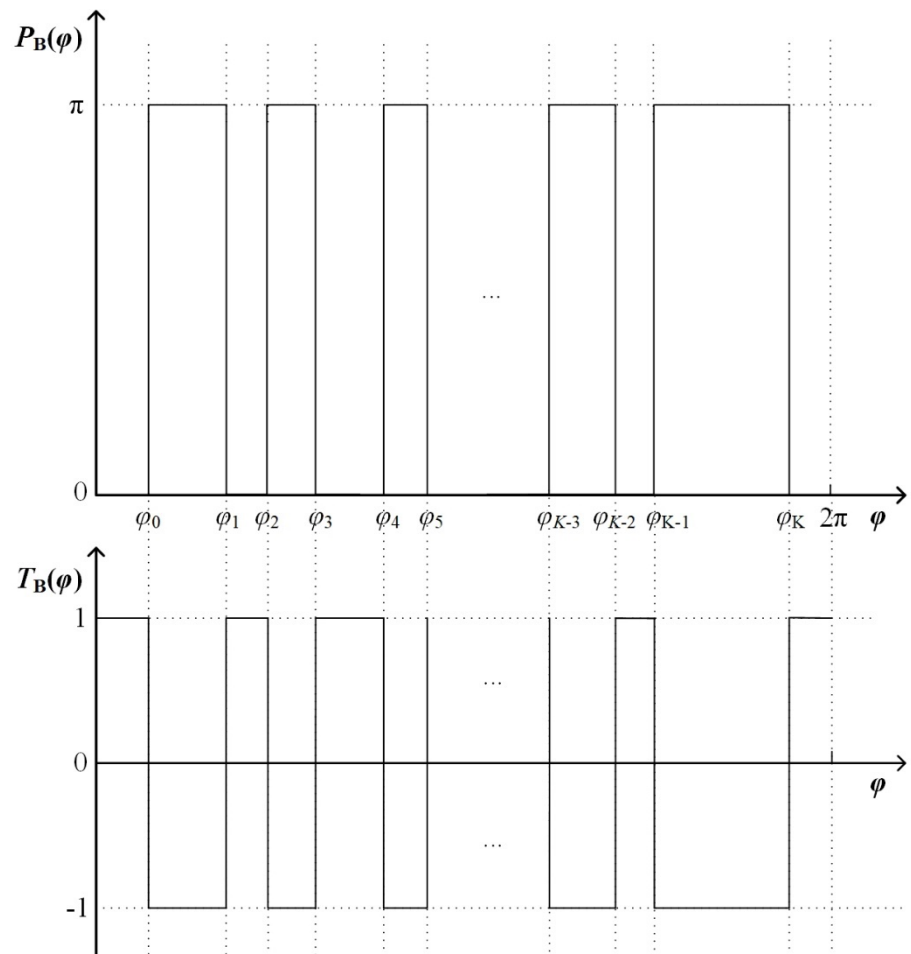


Fig. S1. The phase distribution of an azimuthal binary phase grating

In Fig. S1, φ is the azimuthal angle, $\{\varphi_\kappa\}$ denotes the azimuthal transition points in one grating period (2π) with $\kappa=0, 1, 2, \dots, K$. For a rectangular element, taking $[\varphi_0, \varphi_1]$ as an example, its phase distribution is:

$$P_1(\varphi)=\pi \cdot \text{rect}\left[\frac{\varphi-(\varphi_0+\varphi_1)/2}{\varphi_1-\varphi_0}\right], \varphi \in [0, 2\pi) \quad (\text{S1})$$

Eq. (2) has already given the phase distribution of an azimuthal binary phase. Actually, from Eq. (S1), it can also be expressed as the superposition of a series of rectangular impulses, and thus Eq. (2) turns to:

$$P_B(\varphi)=\pi \sum_{m=1}^{(K-1)/2} \text{rect}\left[\frac{\varphi-0.5(\varphi_{2m-2}+\varphi_{2m-1})}{\varphi_{2m-1}-\varphi_{2m-2}}\right], \varphi \in [0, 2\pi) \quad (\text{S2})$$

Thus, its transmittance function reads:

$$T_B(\varphi)=\exp[iP_B(\varphi)] \quad (\text{S3})$$

Fig.S1 has clearly illustrated the corresponding relationship between the transmittance and the phase distributions. When $P_B(\varphi)=0$, $T_B(\varphi)=\exp(i \cdot 0)=1$; when $P_B(\varphi)=\pi$, $T_B(\varphi)=\exp(i \cdot \pi)=-1$. Similar to the phase distribution, the transmission function of the grating is also in the form of rectangular wave, which can be expressed by scaling, flipping and translating the phase distribution function as:

$$T_B(\varphi)=1-\frac{2}{\pi}P_B(\varphi) \quad (\text{S4})$$

According to the linear property of the Fourier transform, $\mathcal{F}\{T_B(\varphi)\}=\mathcal{F}\{1\}-2/\pi \cdot \mathcal{F}\{P_B(\varphi)\}$. Thus, the Fourier transform of $T_B(\varphi)$ can be divided into two parts, as the Fourier transform of 1 and $P_B(\varphi)$ respectively:

$$\mathcal{F}\{1\}=2\pi\delta(l) \quad (\text{S5})$$

$$\mathcal{F}\{P_B(\varphi)\}=\sum_{m=1}^{(K-1)/2} \frac{(\varphi_{2m+1}-\varphi_{2m})}{2} \sum_{l=-\infty}^{\infty} \left\{ \text{sinc}[0.5(\varphi_{2m+1}-\varphi_{2m})l] \exp[-il \cdot 0.5(\varphi_{2m}+\varphi_{2m+1})] \right\} \exp(il\varphi) \quad (\text{S6})$$

where $l \in \mathbf{Z}$ and represents the OAM eigen value. $\delta(l)$ stands for the Delta function, and sinc function is $\text{sinc}(x)=\sin(\pi x)/(\pi x)$. Then from Eq. (S4) to Eq. (S6), the transmittance of the grating can be Fourier expanded as:

$$\begin{aligned} \mathcal{F}\{T_B(\varphi)\} &= \frac{1}{\pi} \sum_{m=1}^{(K-1)/2} (\varphi_{2m}-\varphi_{2m+1}) \sum_{l=-\infty}^{\infty} \left\{ \text{sinc}[0.5(\varphi_{2m+1}-\varphi_{2m})l] \exp[-il \cdot 0.5(\varphi_{2m}+\varphi_{2m+1})] \right\} \exp(il\varphi) \\ &\quad + 2\pi\delta(l), \varphi \in [0, 2\pi) \end{aligned} \quad (\text{S7})$$

From Eq. (S7), the far-field diffraction comprises multiple OAM modes $\exp(il\varphi)$, with corresponding complex amplitude:

$$\sum_{m=1}^{(K-1)/2} (\varphi_{2m}-\varphi_{2m+1}) \left\{ \text{sinc}[0.5(\varphi_{2m+1}-\varphi_{2m})l] \exp[-il \cdot 0.5(\varphi_{2m}+\varphi_{2m+1})] \right\} \quad (\text{S8})$$

which is the function of azimuthal transition points $\{\varphi_\kappa\}$. Eq. (S8) imply the finally generated OAM spectrum is determined only by the number and value of azimuthal transition points.

Supplementary Note 2: Helical harmonic decomposition

Due to the azimuthally periodic distributions of helical harmonic, a beam $E(r, \varphi)$ under polar coordinate can be expanded directly through helical harmonics $\exp(il\varphi)$ as [42,48,49]:

$$E(r,\varphi)=\frac{1}{\sqrt{2\pi}}\sum_{l=-\infty}^{+\infty}a_l\exp(il\varphi) \quad (\text{S9})$$

with the complex coefficient a_l :

$$a_l=\frac{1}{\sqrt{2\pi}}\int_0^{2\pi}E(r,\varphi)\exp(-il\varphi)d\varphi \quad (\text{S10})$$

The parameter a_l comprises the amplitude and initial phase of l -th OAM components. Hence $|a_l|^2$ corresponds to the intensity of OAM channel l and constitutes the OAM spectrum $\{|a_l|^2\}$. Considering the relationship given in Eqs. (S8)-(S10), one can establish the function between the OAM spectrum $\{|a_l|^2\}$ and azimuthal transition points φ_κ as:

$$|a_l|^2=\left|\sum_{m=1}^{(K-1)/2}(\varphi_{2m}-\varphi_{2m+1})\{\text{sinc}[0.5(\varphi_{2m+1}-\varphi_{2m})l]\exp[-il\cdot 0.5(\varphi_{2m}+\varphi_{2m+1})]\}\right|^2 \quad (\text{S11})$$

Supplementary Note 3: Transition points mapping

A phase-only grating with periodical varying binary phases along x or y directions in Cartesian coordinates, also known as Dammann grating, can divide an incident beam into multiple beams with equal intensities and identical interval angles, thus form a beam array [50,51]. In other words, lateral $0-\pi$ binary phase induces the spatial expansion of the incident beam, namely, the superposition of several orders (diffraction order) in “ x -space”. There are many transition points x_κ (boundary points separating phase values 0 and π) in each grating period, and featured the transmittance function within the unit grating period as:

$$T_B(x)=\pi\sum_{\kappa=1}^K(-1)^{\kappa-1}\text{rect}\left(\frac{x}{x_\kappa}-0.5\right), x\in[0,1) \quad (\text{S12})$$

From a mathematical point of view, Eq. (2) in the main text is essentially the same as that described in Equation (S12). Their difference reflects on the independent variables under various coordinates. Therefore, mapping the lateral transition points into azimuth contributes to similar effect as expanding the incident mode along azimuthal angle and forming the superposition of multiple azimuthal modes with equal intensities, namely, the OAM comb.

In 1995, C. Zhou et al. have already studied the lateral transition points to produce 1 dimensional spatial beam array [43], where numerical solutions of optimal lateral transition points $\{x_\kappa\}$ within one unit grating period for various cases are proposed. For the azimuthal binary phase here, the azimuthal grating period is fixed as 2π . Additionally, the azimuthal angle φ varies uniformly along the azimuthal coordinate. Thus, the mapping can be accomplished easily through multiplying 2π , as $\varphi_\kappa=2\pi x_\kappa$.

Table S1 lists some of the azimuthal transition points, OAM distributions, uniformities U and efficiencies η of their corresponding generated OAM combs. Note that azimuthal transition points for generating OAM combs with mode interval $\Delta l \neq 1$ is derived through scaling the azimuthal angle φ .

Table S1. Some of the azimuthal transition points and their corresponding OAM combs.

Azimuthal transition points $\{\varphi_\kappa\}$	OAM components $\{l\}$	Uniformity U	Efficiency η
0, 3.1416	-1, +1	99.96%	80.70%
0, 1.5708, 3.1416, 4.7124	-2, +2	99.99%	80.32%

0, 0.6283, 1.2566, 1.8850, 2.5133, 3.1416, 3.7699, 4.3982, 5.0265, 5.6549	-5, +5	99.95%	83.31%
0, 4.6200	-1, 0, +1	99.44%	63.03%
0, 0.2425, 2.4555, 4.1186	-2, -1, 0, +1, +2	99.07%	76.27%
0, 1.5399, 2.0944, 3.6343, 4.1888, 5.7287	-3, 0, +3	99.49%	60.19%
0, 1.3859, 2.8000, 3.1416, 4.5275, 5.9416	-3, -1, +1, +3	99.80%	74.55%
0, 0.6929, 1.4000, 1.5708, 2.2637, 2.9708, 3.1416, 3.8345, 4.5416, 4.7124, 5.4053, 6.1124	-6, -2, +2, +6	99.51%	73.96%
0, 0.7286, 1.3358, 1.6516, 3.1416, 3.8702, 4.4774, 4.7932	-6, -4, -2, 0, +2, +4, +6	98.80%	82.49%
0, 0.4190, 0.8087, 1.7963, 2.8693, 3.7127	-4, -3, -2, -1, 0, +1, +2, +3, +4	99.61%	78.32%

Supplementary Note 4: Simulation of far-field diffraction of azimuthal binary phase

The numerical simulation of far-field diffraction of azimuthal binary phase with incident Gaussian beams is based on the diffraction integral formula from scalar diffraction theory. Here Fresnel diffraction is chosen to simplify the diffraction integral formula under paraxial approximation. However, it may cause some problems, since Fresnel diffraction is not applicable in the calculation of the far-field diffraction but is good for the finite propagation distance. So here we have to bring in a Fourier lens in the diffraction path to address such issue, since the pattern on the back focal plane of the lens is the zoomed far-field diffraction patterns indeed.

The transmittance function of a Fourier lens under Cartesian coordinates (x,y) is:

$$T_L = \exp\left(ik \cdot \frac{x^2+y^2}{f}\right) \quad (\text{S13})$$

where $k=2\pi/\lambda$ denotes wave number (λ is the wavelength), and f denotes focal length. The Fresnel transmission function is:

$$H_F(x,y,d) = \exp\left[ikd\left(1 - \frac{x^2+y^2}{2d^2}\right)\right] \quad (\text{S14})$$

with d the transmission distance. From Fresnel diffraction integral, the diffraction field of E_0 after d distance transmission reads [52]:

$$E_d = \mathcal{F}^{-1}[\mathcal{F}(E_0) \cdot H_F] \quad (\text{S15})$$

where \mathcal{F} and \mathcal{F}^{-1} are Fourier transform and Fourier inversion respectively. Equation (S15) allows us to use fast Fourier transform (FFT) to analyze the diffraction, and will make the calculation easier.

From the principle of Fourier optics, a plano-convex lens, namely the Fourier lens, should be placed behind the azimuthal binary phase grating at the position of the focal length f . Therefore, the field E_F on the lens plane should be calculated firstly through Eqs. (S14) & (S15) with the transmission distance $d=f$ and reads:

$$E_F = \mathcal{F}^{-1}[\mathcal{F}(GT_B) \cdot H_F(f)] \quad (\text{S16})$$

where G and T_B denote the complex amplitude of a Gaussian beam and the transmittance function of the azimuthal binary phase respectively. Then introducing the lens and the finally obtained far-

field diffraction E at the back focal plane is:

$$E = \mathcal{F}^{-1}[\mathcal{F}(E_F T_L) \cdot H_F(f)] \quad (\text{S17})$$

Supplementary Note 5: Experiment setup

An experimental setup, as sketched in Fig. S2, is built to show the performance of OAM comb generation through azimuthal binary phases. A 1.6 μm distributed feedback (DFB) laser diode is employed as the source. The DFB laser beam is transmitted through a single mode fiber (SMF) and coupled into free-space with 3 mm diameter through a collimator. After passing through a polarized beam splitter (PBS), the Gaussian beam turns into horizontally linear polarization, thus to satisfy the demand of phase-only modulation of the liquid-crystal spatial light modulator (SLM) (Holoeye, PLUTO-TELCO-013-C). The phase distribution of the proposed azimuthal binary phase is encoded on the SLM to produce desired OAM combs. The far-field diffraction patterns are observed through an infrared charge coupled device (CCD) camera accompanied with a plano-convex lens (PCL). Note that both of distances from SLM to PCL and from PCL to CCD, are fixed as the focal length of the PCL as $f=200$ mm.

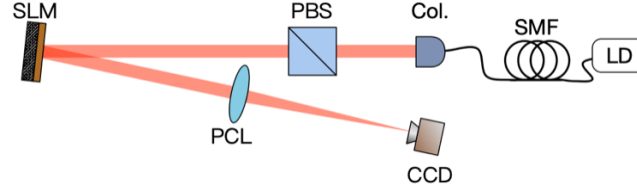


Fig. S2. Experimental setup. DFB, distributed feedback laser diode. SLM, single mode fiber. Col., collimator. PBS, polarized beam splitter. SLM, liquid-crystal spatial light modulator. PCL, plano-convex lens. CCD, infrared CCD camera.

Supplementary Note 6: Azimuthal transition points in the experiment

In the presented proof-of-principle experiment, two OAM combs are generated. This note gives the azimuthal transition points for generating the two OAM combs.

(1) OAM comb 1: OAM states range: $-63 \sim +63$, OAM mode interval $\Delta l=2$.

$\{\varphi_k\}$ consists of 70 azimuthal transition points:

{0, 0.0654, 0.1095, 0.1854, 0.2550, 0.2996, 0.3825, 0.4433, 0.5277, 0.6118, 0.6456, 0.8074, 0.9000, 1.3369, 1.5495, 1.6505, 1.7605, 1.8155, 1.8639, 1.9960, 2.0368, 2.1219, 2.2730, 2.4053, 2.4895, 2.5937, 2.6624, 2.7229, 2.7530, 2.8186, 2.8867, 2.9336, 2.9799, 3.0406, 3.0747, 3.1416, 3.2070, 3.2511, 3.3270, 3.3966, 3.4412, 3.5241, 3.5849, 3.6693, 3.7534, 3.7872, 3.9490, 4.0416, 4.4785, 4.6911, 4.7921, 4.9021, 4.9571, 5.0055, 5.1376, 5.1784, 5.2635, 5.4146, 5.5469, 5.6311, 5.7353, 5.8040, 5.8645, 5.8946, 5.9602, 6.0283, 6.0752, 6.1215, 6.1822, 6.2163}

(2) OAM comb 2: OAM states range: $-62 \sim +62$, OAM mode interval $\Delta l=4$.

$\{\varphi_k\}$ consists of 68 azimuthal transition points:

{0, 0.1740, 0.2796, 0.3459, 0.4191, 0.5441, 0.6151, 0.6626, 0.7245, 0.7813, 1.0370, 1.0939, 1.2598, 1.3609, 1.3858, 1.4618, 1.5205, 1.5708, 1.7448, 1.8504, 1.9167, 1.9899, 2.1149, 2.1859, 2.2334, 2.2952, 2.3521, 2.6078, 2.6647, 2.8306, 2.9317, 2.9566, 3.0326, 3.0913, 3.1416, 3.3156, 3.4212, 3.4875, 3.5607, 3.6857, 3.7567, 3.8042, 3.8660, 3.9229, 4.1786, 4.2355, 4.4014, 4.5025, 4.5273, 4.6034, 4.6621, 4.7124, 4.8864, 4.9920, 5.0583, 5.1315, 5.2565, 5.3275, 5.3750, 5.4368, 5.4937, 5.7494, 5.8063, 5.9722, 6.0733, 6.0981, 6.1742, 6.2329}

Supplementary Note 7: Experimental OAM spectrum analyzing

For the sake of simplicity, when measuring the OAM spectrum of the produced OAM comb, a series of spiral phases are encoded simultaneously with the azimuthal binary phase. Then a series of corresponding back-converted patterns are captured by the CCD. The principle of back-conversion method can be understood as, if a $-l$ -th order spiral phase is encoded, the OAM state l in the OAM comb turns to $l-l=0$, thus a bright spot emerges at the beam center. However, the other OAM states l_0 turns to $l_0-l \neq 0$, and won't concentrate to the center. Therefore, by measuring the intensity of the bright spot in each back-converted pattern, one can acquire the OAM spectrum.

Fig. S3 displays some of the experimentally captured back-converted patterns for the second generated OAM comb (l range $-62 \sim +62$, $\Delta l=4$). The orders of the back-converting spiral phases are also labeled. The green dashed circle in each inset is the sampling area, where intensities inside it are regarded as the back-converted OAM channel. Note that the sampling area is selected as covering the entire bright spots of fundamental mode. Its size and position are fixed for all the back-converted patterns in analyzing one OAM comb. In addition, no optical power meters are employed here. The main feature of an OAM comb is the relative intensity among each OAM channels. The sum of every pixel's gray value of the patterns received by the CCD camera is proportional to the real intensity of the incident beams when the received power is lower than the camera's threshold [53]. Hence here the sum of pixel gray values inside the sampling area, which is obtained through image processing, is employed to represent the relative intensity indirectly. Note that the method of OAM spectrum measurement is diversiform, schemes like log-polar coordinate transformer [54] and rotational Doppler effect [55] is also feasible here.

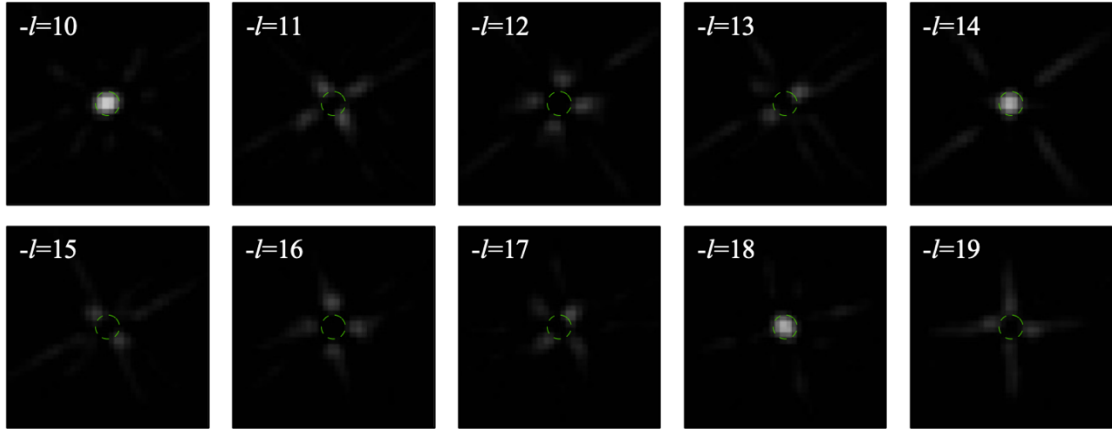


Fig. S3. Experimental back-converted patterns. Some of the experimental back-converted patterns of the generated OAM comb with l range $-62 \sim +62$ and $\Delta l=4$ are listed. The green dashed circle in each inset shows the sampling area.